AN EFFICIENT METHOD FOR VESSEL WIDTH MEASUREMENT ON COLOR RETINAL IMAGES

Alauddin Bhuiyan, Baikunth Nath, Joselito Chua and Kotagiri Ramamohanarao
Department of Computer Science and Software Engineering and NICTA Victoria Research Laboratory
The University of Melbourne, Australia

Keywords: Microvascular Sign, Gradient Operator, Adaptive Region Growing Technique, Texture Classification, Gabor Energy Filter Bank, Fuzzy C-Means Clustering.

Abstract: Vessel diameter is an important factor for indicating retinal microvascular signs. In automated retinal image analysis, the measurement of vascular width is a complicated process as most of the vessels are few pixels wide. In this paper, we propose a new technique to measure the retinal blood vessel diameter which can be used to detect arteriolar narrowing, arteriovenous (AV) nicking, branching coefficients, etc. to diagnose related diseases. First, we apply the Adaptive Region Growing (ARG) segmentation technique to obtain the edges of the blood vessels. Following that we apply the unsupervised texture classification method to segment the blood vessels from where we obtain the vessel centreline. Then we utilize the edge image and vessel centreline image to obtain the potential pixels pairs which pass through a centreline pixel. We apply a rotational invariant mask to search the pixel pairs from the edge image. From those pixels we calculate the shortest distance pair which will be the vessel width for that cross-section. We evaluate our technique with manually measured width for different vessels' cross-sectional area and achieve an average accuracy of 95.8%.

1 INTRODUCTION

Accurate measurement of retinal vessel diameter is an important part in the diagnosis of many diseases. A variety of morphological changes occur to retinal vessels in different disease conditions. The change in width of retinal vessels within the fundus image is believed to be indicative of the risk level of diabetic retinopathy; venous beading (unusual variations in diameter along a vein) is one of the most powerful predictor of proliferate diabetic retinopathy. Generalized and focal retinal arteriolar narrowing and arteriovenous nicking have been shown to be strongly associated with current and past hypertension reflecting the transient and persistent structural effects of elevated blood pressure on the retinal vascular network. In addition, retinal arteriolar bifurcation diameter exponents have been shown to change significantly in patients with peripheral vascular disease and arteriosclerosis and a variety of retinal microvascular abnormalities have been shown to relate to the risk of stroke (Lowell et al., 2004). Therefore, an accurate measurement of vessel diameter and geometry is necessary for effective diagnosis of such diseases.

The measurement of the vascular diameter is critical and a challenging task whose accuracy depends on the accuracy of the segmentation method. A review for the blood vessel segmentation is provided in the literature (Bhuiyan et al., 2007a). The study of vessel diameter measurement is still an open area for improvement. Zhou et al. (Zhou et al., 1994) have applied a model-based approach for tracking and to estimating widths of retinal vessels. Their model assumes that image intensity as a function of distance across the vessel displays a single Gaussian form. However, high resolution fundus photographs often display a central light reflex (Brinchman-hansan and Heier, 1986). Intensity distribution curves is not always of single Gaussian form, so that using a single Gaussian model for simulating intensity profile of vessel could produce poor fits and subsequently provide inaccurate diameter estimations (Gao et al., 2001). Gao et al. (Gao et al., 2001) model the intensity profiles over vessel cross section using twin Gaussian functions to acquire vessel width. This technique may produce poor results in case of minor vessels where the contrast is less. Lowell et al. (Lowell et al., 2004) have proposed an algorithm based on fitting a local 2D vessel model, which can measure vascular width to an accuracy of about one third of

Bhuiyan A., Nath B., Chua J. and Ramamohanarao K. (2008).
AN EFFICIENT METHOD FOR VESSEL WIDTH MEASUREMENT ON COLOR RETINAL IMAGES.
In *Proceedings of the First International Conference on Bio-inspired Systems and Signal Processing*, pages 178-185
DOI: 10.5220/0001059401780185

a pixel. However, the technique is biased on smooth data (image) and suffers from measuring the width of minor vessels where the contrast is very less.

In this paper, we introduce a new algorithm, based on vessel centreline and edges information. We apply the adaptive region growing technique to segment the vessels edges (Bhuiyan et al., 2007a) and the unsupervised texture classification method to segment the vessels and detect the centreline (Bhuiyan et al., 2007b). For each selected centerline pixel we map the edge image of the retinal vessels edge pixels and find all the potential line end points or pairing pixels on opposite edge passing through this centreline pixels. From these potential lines we find the line that has the minimum length and consider this as the vessel width for that cross-sectional area. In this way, we can measure the width of the blood vessel continuing through the centreline of all the vessels. A specific feature of our technique is that it can calculate the vessel width when it is one pixel wide.

The rest of the paper is organized as follows: Section 2 introduces the proposed method of blood vessel width measurement. Edge based blood vessel segmentation technique is described in section 3. Section 4 illustrates the vessel centreline detection procedure. The vessel width measurement method is described in section 5. The experimental results are provided in section 6 and finally the conclusion and future research directions are drawn in section 7

2 PROPOSED METHOD

We propose the blood vessels' width measurement algorithm based on the vessel edge and centreline. The major advantage of our technique is that it is less sensitive to noise and work equally for the low contrast vessels (particularly for minor vessels). We adopt two segmented images that are produced from the original RGB image. At first, we apply the ARG segmentation technique to obtain the vessel edges, then we apply the unsupervised texture classification method to segment the blood vessels from where we obtain the vessel centreline. We map the vessel centreline image and pick any of the vessel centreline pixel. For that particular pixel we apply a rotational invariant mask whose centre is that pixels position and searches the potential pixels from the edge image using a continuous increment of lower to higher distance and orientation. For each case, if the gray scale value of that pixel position is 255 or white it finds the mirror of this pixel by searching through a fixed angle (exactly incrementing 180 degree) but in variable distance. This is to give the flexibility and consistency to our method as the centreline pixels may not be in the exact position of vessel centre. In this way, we can obtain all the potential pairs (line end points) which pass through that centreline pixel. From those pairs we calculate the minimum distance/length pair which is the width of that cross-section of the blood vessel. Figure 1 depicts the overall technique of our proposed method.

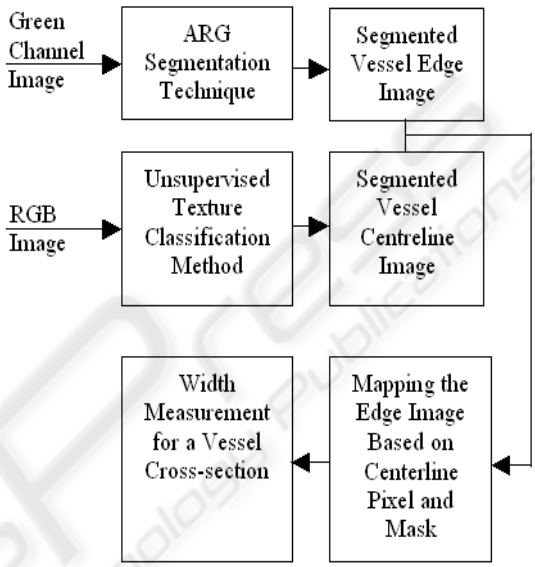

Figure 1: The overall system for measuring blood vessel width.

3 VESSEL EDGE DETECTION

We implemented the vessel segmentation technique based on vessel edges. In the following subsections we provide a brief illustration of this method.

3.1 Preprocessing of Retinal Image

Adaptive Histogram Equalization (AHE) method is implemented, using MATLAB, to enhance the contrast of the image intensity by transforming the values using contrast-limited adaptive histogram equalization (Figure 2).

3.2 Image Conversion

The enhanced retinal image is converted into gradient image (Figure 2) using first order partial differential operator. The gradient of an image $f(x,y)$ at location (x,y) is defined as the two dimensional vector (Gon-

zalez and Wintz 1987)

$$G[f(x,y)] = [G_x, G_y] = \left[\frac{\partial f}{\partial x}, \frac{\partial f}{\partial y}\right] \quad (1)$$

For edge detection, we are interested in the magnitude $G[f(x,y)]$ and direction $\alpha(x,y)$of the vector, generally referred to simply as the gradient and denoted and commonly takes the value of

$$\begin{aligned} G[f(x,y)] &\approx |G_x| + |G_y| \\ \alpha(x,y) &= \tan^{-1}(G_y/G_x) \end{aligned} \quad (2)$$

where the angle is measured with respect to the x axis.

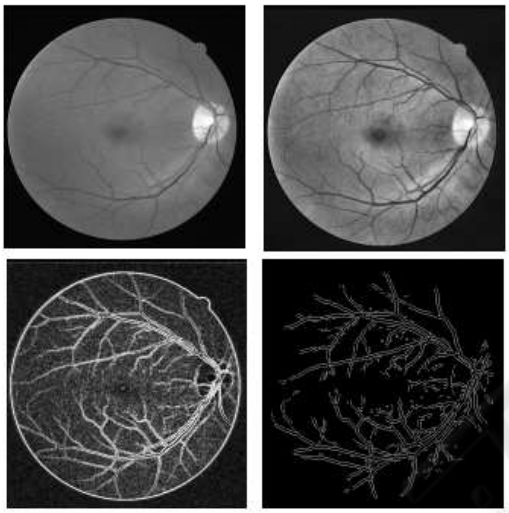

Figure 2: Original retinal image, its Adaptive Histogram Equalized image (top; left to right), the Gradient Image and final ARG output image (bottom; left to right).

3.3 Adaptive Region Growing Technique

The edges of vessels are segmented using region growing procedure (Gonzalez et al., 2004) that groups pixels or sub regions into larger regions based on gradient magnitude. As the gradient magnitude is not constant for the whole vessel we need to consider an adaptive gradient value that gradually increases or decreases to append the pixel to a region. We call it an adaptive procedure, as the difference of neighboring pixels intensity value is always adapted for the region growing process. The region growing process starts with appending the pixels that pass certain threshold value. For region growing we find the intensity difference between a pixel belonging to a region and its neighboring potential region growing pixels. The pixel is considered for appending in that region if the difference is less than a threshold value. The threshold value is calculated by considering the maximum differential gradient magnitude for any neighboring pixels with equal (approximately) gradient direction. Region growing should stop when no more pixels satisfy the criteria for inclusion in that region. In the region growing process each region is labeled with a unique number. For that purpose we construct a cell array with region number and its pixel position. The image is scanned in a row-wise manner until its end, and each pixel that satisfies our criteria is taken into account for growing a region with its 8-neighborhood connectivity.

3.4 Parallel Region Detection

We calculate the parallel edges (regions) by considering pixel orientation belonging to each region. At first, we pick the region number and belonging pixel coordinates from the constructed cell array. Then we grouped the region/regions parallel to each region, which is calculated by mapping the pixels gradient direction. For each region every pixel is searched from its potential parallel region and once a maximum number of pixels match with the other region we consider it as parallel to that region. We consider all regions and once a region is considered we assigned a flag value to that region so that it will not be considered again. In this way we can only filter the vessels from the region and discard all other regions, which are background noise or other objects like haemorrhage, macula, etc in the retinal image.

3.5 Experimental Results

We considered DRIVE database (DRIVE-database, 2004) and applied our technique on five images for initial assessment. For performance evaluation we employed an expert to find the number of vessels in the original image and detected output image (Figure 2). We achieved an overall 94.98% detection accuracy.

4 VESSEL CENTRELINE DETECTION

We implemented the unsupervised texture classification based vessel segmentation method from which we detect the vessel centreline. We consider Gaussian and $L^*a^*b^*$ perceptually uniform color spaces with the original RGB image for texture feature extraction. To extract features, a bank of Gabor energy filters with three wavelengths and twenty-four orientations is applied in each selected color channel. Then

a texture image is constructed from the maximum response of all orientations for a particular wavelength in each color channel. From the texture images, a feature vector is constructed for each pixel. These feature vectors are classified using the Fuzzy C-Means (FCM) clustering algorithm. Finally, we segment the image based on the cluster centroid value.

4.1 Color Space Transformation and Preprocessing

Generally image data is given in RGB space (because of the availability of data produced by the camera apparatus). The definition of $L^*a^*b^*$ is based on an intermediate system, known as the CIE XYZ space (ITU-Rec 709). This space is derived from RGB as below (Wyszecki and Stiles, 1982)

$$\begin{aligned} X &= 0.412453R + 0.357580G + 0.180423B \\ Y &= 0.212671R + 0.715160G + 0.072169B \\ Z &= 0.019334R + 0.119193G + 0.950227B \end{aligned} \tag{3}$$

$L^*a^*b^*$ color space is defined as follows:

$$\begin{aligned} L^* &= 116 f(Y/Y_n) - 16 \\ a^* &= 500[f(X/X_n) - f(Y/Y_n)] \\ b^* &= 200[f(Y/Y_n)] - f(Z/Z_n) \end{aligned} \tag{4}$$

where $f(q) = q^{1/3}$ if $q < 0.008856$ and is constant 7.87+16/116 otherwise. X_n, Y_n and Z_n represent a reference white as defined by a CIE standard illuminant, D_{65} in this case. This is obtained by setting $R = G = B = 100$ in (1), $q \in \{X/X_n, Y/Y_n, Z/Z_n\}$.

Gaussian color model can also be well approximated by the RGB values. The first three components $\hat{E}$, $\hat{E_\lambda}$ and $\hat{E_{\lambda\lambda}}$ of the Gaussian color model (Taylor expansion of the Gaussian weighted spectral energy distribution at Gaussian central wavelength and scale) can be approximated from the CIE 1964 XYZ basis when taking $\lambda_0 = 520nm$ (Gaussian central wavelength) and $\sigma_\lambda = 55nm$ (scale) as follows (Geusebroek et al., 2001)

$$\begin{pmatrix} \hat{E} \\ \hat{E_\lambda} \\ \hat{E_{\lambda\lambda}} \end{pmatrix} = \begin{pmatrix} -0.48 & 1.2 & 0.28 \\ 0.48 & -0.4 & -0.4 \\ 1.18 & -1.3 & 0 \end{pmatrix} \begin{pmatrix} X \\ Y \\ Z \end{pmatrix} \tag{5}$$

The product of (3) and (5) gives the desired implementation of the Gaussian color model in RGB terms (Figure 3). The Adaptive Histogram Equalization method was implemented, using MATLAB, to enhance the contrast of the image intensity.

4.2 Texture Feature Extraction

Texture generally describes second order property of surfaces and scenes, measured over image intensities.

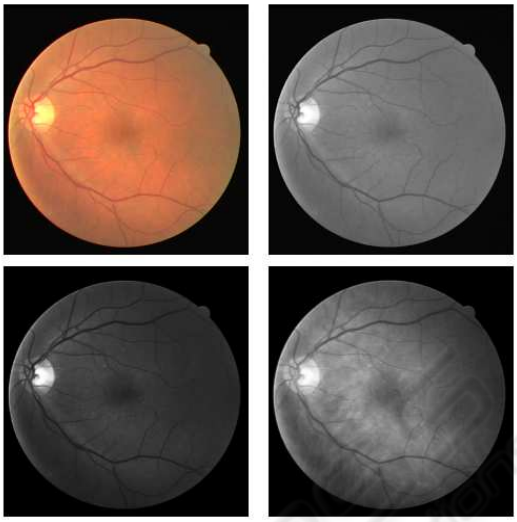

Figure 3: Original RGB and its Green channel image (top; left to right), Gaussian transformed first and second component image (bottom; left to right).

A Gabor filter has weak responses along all orientations on the smooth (background) surface. On the other hand, when it positioned on a linear pattern object (like a vessel) the Gabor filter produces relatively large differences in its responses when the orientation parameter changes (Wu et al., 2006). Hence, the use of Gabor filters to analyze the texture of the retinal images is very promising. In the following two subsections we illustrate the Gabor filter based texture analysis method.

4.2.1 Gabor Filter

An input image $I(x,y)$, $(x,y) \in \Omega$ where Ω is the set of image points, is convolved with a 2D Gabor function $g(x,y)$, $(x,y) \in \omega$, to obtain a Gabor feature image $r(x,y)$ (Gabor filter response) as follows (Kruizinga and Petkov, 1999)

$$r(x,y) = \iint_{\Omega} I(\xi,\eta) g(x-\xi, y-\eta) d\xi d\eta \tag{6}$$

We use the following family of 2D Gabor functions to model the spatial summation properties of an image (Kruizinga and Petkov, 1999)

$$\begin{aligned} g_{\xi,\eta,\lambda,\Theta,\phi}(x,y) &= \exp\left(-\tfrac{x'^2+\gamma^2 y'^2}{2\sigma^2}\right)\cos\left(2\pi\tfrac{x'}{\lambda}+\phi\right) \\ x' &= (x-\xi)\cos\Theta - (y-\eta)\sin\Theta \\ y' &= (x-\xi)\cos\Theta - (y-\eta)\sin\Theta \end{aligned} \tag{7}$$

where the arguments x and y specify the position of a light impulse in the visual field and $\xi, \eta, \sigma, \gamma, \lambda, \Theta, \phi$ are parameters. The pair (ξ, η) specifies the center of a receptive field in image coordinates. The standard

deviation σ of the Gaussian factor determines the size of the receptive filed. Its eccentricity is determined by the parameter γ called the spatial aspect ratio. The parameter λ is the wavelength of the cosine factor which determines the preferred spatial frequency $\frac{1}{\lambda}$ of the receptive field function $g_{\xi,\eta,\lambda,\Theta,\phi}(x,y)$. The parameter Θ specifies the orientation of the normal to the parallel excitatory and inhibitory stripe zones - this normal is the axis x' in (5). Finally, the parameter $\phi \in (-\pi,\pi)$, which is a phase offset argument of the harmonic factor $\cos(2\pi\frac{x'}{\lambda}+\phi)$, determines the symmetry of the function $g_{\xi,\eta,\lambda,\Theta,\phi}(x,y)$.

4.2.2 Gabor Energy Features

A set of textures was obtained based on the use of Gabor filters (6) according to a multichannel filtering scheme. For this purpose, each image was filtered with a set of Gabor filters with different preferred orientation, spatial frequencies and phases. The filter results of the phase pairs were combined, yielding the Gabor energy quantity (Kruizinga and Petkov, 1999):

$$E_{\xi,\eta,\Theta,\lambda} = \sqrt{r^2_{\xi,\eta,\Theta,\lambda,0} + r^2_{\xi,\eta,\Theta,\lambda,\pi/2}} \qquad (8)$$

where $r^2_{\xi,\eta,\Theta,\lambda,0}$ and $r^2_{\xi,\eta,\Theta,\lambda,\pi/2}$ are the outputs of the symmetric and antisymmetric filters. We used Gabor energy filters with twenty-four equidistant preferred orientations ($\Theta = 0,15,30,..,345$) and three preferred spatial frequencies ($\lambda = 6,7,8$). In this way an appropriate coverage was performed of the spatial frequency domain.

We considered the maximum response value per pixel on each color channel to reduce the feature vector length and complexity of training on data for the classifier. In addition, we constructed an image (Figure 4) on each color channel which was used for histogram analysis to determine the cluster number. From these images we constructed twelve element length feature vector for each pixel in each retinal image to classify them into vessel and non-vessel using the FCM clustering algorithm.

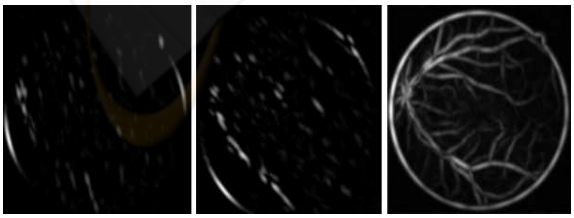

Figure 4: Texture analyzed image with the orientations of 15, 45 degrees and maximum response of all twenty-four orientations (left to right).

4.3 Texture Classification and Image Segmentation

The FCM is a data clustering technique where in each data point belongs to a cluster to some degree that is specified by a membership grade. Let $X = x_1, x_2, , x_N$ where $x \in R^N$ present a given set of feature data. The objective of the FCM clustering algorithm is to minimize the Fuzzy C-Means cost function formulated as (Bezdek, 1981)

$$J(U,V) = \sum_{j=1}^{C}\sum_{i=1}^{N}(\mu_{ij})^m ||x_i - v_j||^2 \qquad (9)$$

$V = \{v_1, v_2, , v_C\}$ are the cluster centers. $U = (\mu_{ij})_{N\times C}$ is fuzzy partition matrix, in which each member is between the data vector x_i and the cluster j. The values of matrix U should satisfy the following conditions:

$$\mu_{ij} \in [0,1], i = 1,..,N, j = 1,..,C \qquad (10)$$

$$\mu_{ij} = 1, i = 1,..,N \qquad (11)$$

The exponent $m \in [1,\infty]$ is the weighting exponent, which determines the fuzziness of the clusters. The most commonly used distance norm is the Euclidean distance $d_{ij} = ||x_i - v_j||$.

We used the Matlab Fuzzy Logic Toolbox for clustering 253440 vectors (the size of the retinal image is 512x495) in length twelve for each retinal image. In each retinal image clustering procedure, the number of clusters was assigned after analyzing the histogram of the texture image. The parameter values used for the FCM clustering were as follows. The exponent value of 2 for the partition matrix, maximum number of iterations was set to 1000 for the stopping criterion and the minimum amount of improvement being 0.00001. We received the membership values on each cluster for every vector, from which we picked the cluster number that belonged to the highest membership value for each vector and converted it into a 2D matrix. From this matrix we produced the binary image considering the cluster central intensity value which identifies the blood vessels only.

4.4 Experimental Results

Using the DRIVE database (DRIVE-database, 2004) we applied our method on five images for vessel segmentation. For performance evaluation, we detected the vessel centerline in our output segmented images and hand-labeled ground truth segmented (GT) images applying the morphological thinning operation (Figure 5). We achieved an overall 84.37% sensitivity ($TP/(TP+FN)$) and 99.61% specificity ($TN/(TN+FP)$) where TP, TN, FP and FN are true

positive, true negative, false positive and false negative respectively. Hoover et al. (Hoover et al., 2000) method on the same five segmented images provided in 68.23% sensitivity and 98.06% specificity. Clearly, our method produces superior results.

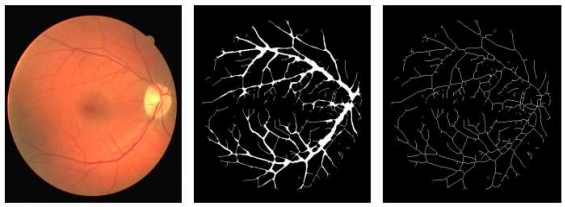

Figure 5: Original RGB image, vessel segmented image, and its centreline image (from left to right).

5 VESSEL WIDTH MEASUREMENT

After obtaining the vessels edge image and centreline image, we mapped these images to find the vessel width for a particular vessel centreline pixel position. To do this we first pick a pixel from the vessel centreline image, then we apply a mask considering this centreline pixel as its centre. The purpose of this mask is to find the potential edge pixels (which may fall in width or cross section of the vessels) in any side of that centreline pixel position. Therefore, we will apply the mask to the edge image only. For searching all the pixel positions inside the mask, we calculate the pixel position by shifting by one up to the size of the mask and rotating each position from 0 to 180 degrees at the same time. For increasing the rotation angle we use the step size (depending on the size of the mask) less then 180/(mask length). Therefore, we can access every cell in the mask using this angle.

For each obtained position we search the edge image gray scale value to check whether it is an edge pixel or not. Once we find an edge pixel we then find it's mirror by shifting the angle of 180 degree and increasing the distance from one to the maximum size of the mask (Figure 6). In this way we produce a rotational invariant mask and pick all the potential pixel pairs to find the width or diameter of that cross sectional area.

$$\begin{aligned} x1 &= x' + r * \cos\theta \\ y1 &= y' + r * \sin\theta \end{aligned} \tag{12}$$

where (x',y') is the vessel centreline pixel position, r=1,2,..(mask size)/2 and $\theta = 0,..,180^o$. For any pixel position, if the gray scale value in the edge image is 255 (white or edge pixel) then we find the pixel $(x2,y2)$ in the opposite edge (mirror of this pixel) considering $\theta = (\theta + 180)$ and varying r.

After applying this operation we obtain the pairs of pixels which are on the opposite edges (at line end points) giving imaginary lines passing through the centerline pixels (Figure 6). From these pixels pairs we find the minimum Euclidian distance $\sqrt{(x_1-x_2)^2+(y_1-y_2)^2}$, the width of that crosssection. In this way, we can measure the width for all vessels including the vessels' with one pixel wide (for which we have the edge and the centreline itself).

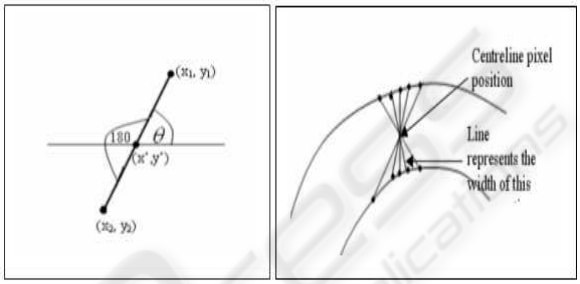

Figure 6: Finding the mirror of an edge pixel(left) and width or minimum distance from potential pairs of pixels (right).

6 EXPERIMENTAL RESULTS AND DISCUSSION

We used the centreline images and edge images for measuring the width of the blood vessels. We measure the accuracy qualitatively by comparing with the width measured by plotting the centreline pixel and its surround edge pixels. We considered ten different vessel cross-sections of these images and observed that our method is working very accurately. Figure 7 portrays the Grid for a cross-section of a blood vessel where c is the centreline pixel and w1 to w8 are potential width end points. Figure 8 depicts the detected width for some cross-sectional points indicating in white lines (enlarged).

	251	252	253	254	255	256	257	258	259	260	261	262	263
455				W8	W7	W6							
456							W5						
457								W4					
458									W3	W2			
459	W1					C					W1		
460		W2											
461			W3	W4									
462					W5	W6							
463							W7						
464								W8					

Figure 7: Grid showing the potential width edge pairs for a cross-section with centreline pixel C.

For quantitative evaluation we considered ten images (each 3072×2048 which captured with the

Table 1: Measuring the accuracy of the automatic width measurement.

Cross-section	Centreline pixel X_c	Y_c	Detected width end points X_1	Y_1	X_2	Y_2	Auto. width (A)	Accuracy (%)	Error (%)
1	2055	629	2068	632	2046	628	22.361	99.14	0.86
2	1859	519	1871	519	1850	520	21.024	97.50	2.50
3	2259	815	2259	811	2259	824	13	99.46	0.54
4	2350	1077	2350	1070	2350	1084	14	87.61	12.39
5	2233	1317	2239	1314	2239	1322	11.314	93.49	6.51
6	2180	1435	2189	1431	2172	1440	19.235	95.39	4.61
7	2045	1451	2055	1452	2042	1452	13	85.55	14.45
8	1683	1500	1691	1509	1680	1496	17.029	87.52	12.48
9	1579	617	608	1593	630	1573	23.409	98.48	1.52
10	1434	855	853	1436	859	1432	7.211	85.48	14.52
11	1443	1000	999	1446	1004	1440	7.81025	91.23	8.77
12	1618	1331	1335	1623	1330	1617	7.81025	89.54	10.46
13	1475	1164	1169	1479	1162	1474	8.6023	83.20	16.80

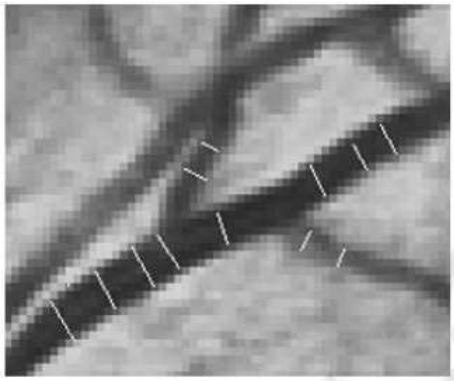

Figure 8: Measured vessel width showing by the white lines in an image portion.

Canon D-60 digital fundus camera) with manually measured width on different cross-sections from Eye and Ear Hospital, Victoria, Australia. For each cross-section, we received the graded width by five different experts who are trained retinal vessel graders of that institution. For manual grading a computer program was used where the graders could zoom in and out at will, moving around the image and selecting various parts. We applied our technique on these images to produce the edge image and vessel centreline image. We considered these images and randomly picked ninety-six cross-sections of vessels varying width from one to twenty-seven pixels. We measured the width for each cross-section by our automatic width measurement technique (we call it automatic width, A) and considered the five manually measured width (we call it manual width) by experts. We calculated the average of the manual width (μ), the standard deviation on manual widths (σ_m) and considered the following formula to find the error,

$$E = \left| \frac{\frac{(\mu-\sigma_m)-A}{(\mu-\sigma_m)} + \frac{(\mu+\sigma_m)-A}{(\mu+\sigma_m)}}{2} \right| = \left| 1 - \frac{\mu \times A}{\mu^2 - \sigma_m^2} \right| \quad (13)$$

In equation (13), we considered $(\mu \pm \sigma_m)$ to normalize it. This formula is a good measure as the error rate will be less if it is within the interval one standard deviation. With this formula, we calculated the error and accuracy in all ninety-six cross-section and achieve an average of 95.8% accuracy (maximum accuracy is 99.58% and minimum accuracy is 83.20%) in the detection of vessel width. We found the maximum error is 16.80% which is 2.04 pixel and the minimum error is 0.698% which is 0.139 pixel. Table 1 and 2 depict the manual and automatic width measurement accuracy on different cross-sections in an image. We compared our technique with (Lowell et al., 2004) which achieved the maximum accuracy of 99% (did not mention the average accuracy for all cross-sections) with minimum pixel error of 0.34. Using the same formula, $|(\mu - A)/\mu|$), we achieved 100% accuracy. Clearly, our technique is performing better.

7 CONCLUSIONS AND FUTURE WORK

In this paper we proposed a new and efficient technique for blood vessels width measurement. This approach is a robust estimator of vessel width in the presence of low contrast and noise. The results obtained are promising and the detected width can be used to measure different parameters (nicking, nar-

Table 2: Manually measured widths for an image cross-sections.

Cross-section	Manually measured width (in Micron) One	Two	Three	Four	Five	Mean width (μ) (in pixel)	Standard Deviation (σ_m)
1	112.42	117.53	107.31	117.53	112.42	22.2	0.8366
2	107.31	112.42	107.31	117.53	107.31	21.6	0.8944
3	66.43	76.65	61.32	71.54	61.32	13.2	1.3088
4	61.32	71.54	61.32	71.54	56.21	12.6	1.3416
5	56.21	66.43	56.21	66.43	66.43	12.2	1.0954
6	107.31	107.31	102.2	102.2	97.09	20.2	0.8366
7	56.21	66.43	45.99	61.32	66.43	11.6	1.6733
8	86.87	107.31	102.2	107.31	97.09	19.6	1.6733
9	132.86	127.75	112.42	132.86	107.31	24	2.3452
10	45.99	51.1	35.77	56.21	35.77	8.8	1.7889
11	40.88	56.21	35.77	45.99	45.99	8.8	1.4832
12	35.77	51.1	45.99	56.21	40.88	9	1.5811
13	35.77	45.99	35.77	45.99	30.66	7.6	1.3416

rowing, branching coefficients, etc.) for diagnosing various diseases. Currently, we are working on the blood vessels' bifurcation and cross-over detection where the measured width is contributing as an important information for perceptual grouping process.

ACKNOWLEDGEMENTS

We would like to thank David Griffiths (Research Assistant, The University of Melbourne and Eye and Ear Hospital, Melbourne, Australia) for providing us with the manually measured width images and data.

REFERENCES

Bezdek, J. (1981). Pattern recognition with fuzzy objective function algorithms. *Plenum Press, USA*.

Bhuiyan, A., Nath, B., and Chua, J. (2007a). An adaptive region growing segmentation for blood vessel detection from retinal images. *Second International Conference on Computer Vision Theory and Applications*, pages 404–409.

Bhuiyan, A., Nath, B., Chua, J., and Kotagiri, R. (2007b). Blood vessel segmentation from color retinal images using unsupervised classification. *In the proceedings of the IEEE International Conference of Image Processing*.

Brinchman-hansan, O. and Heier, H. (1986). Theoritical relations between light streak characterstics and optical properties of retinal vessels. *Acta Ophthalmologica*, 179(33).

DRIVE-database (2004). http://www.isi.uu.nl/research/databases/drive/, image sciences institute, university medical center utrecht, the netherlands.

Gao, X., Bharath, A., Stanton, A., Hughes, A., Chapman, N., and Thom, S. (2001). Measurement of vessel diameters on retinal images for cardiovascular studies. *Proceedings of Medical Image Understanding and Analysis*, pages 1–4.

Geusebroek, J., Boomgaard, R. V. D., Smeulders, A. W. M., and Geerts, H. (2001). Color invariance. *IEEE Transactions on Pattern Analysis and Machine Intelligence*, 23(2):1338–1350.

Gonzalez, R. C., Woods, R. E., and Eddins, S. L. (2004). Digital image processing using matlab. *Prentice Hall*.

Hoover, A., Kouznetsova, V., and Goldbaum, M. (2000). Locating blood vessels in retinal images by piece-wise threshold probing of a matched filter response. *IEEE Transactions on Medical Imaging*, 19(3):203–210.

Kruizinga, P. and Petkov, N. (1999). Nonlinear operator for oriented texture. *IEEE Transactions on Image Processing*, 8(10):1395–1407.

Lowell, J., Hunter, A., Steel, D., Basu, A., Ryder, R., and Kennedy, R. L. (2004). Measurement of retinal vessel widths from fundus images based on 2-d modeling. *IEEE Transactions on Medical Imaging*, 23(10):1196–1204.

Wu, D., Zhang, M., and Liu, J. (2006). On the adaptive detetcion of blood vessels in retinal images. *IEEE Transactions on Biomedical Engineering*, 53(2):341–343.

Wyszecki, G. W. and Stiles, S. W. (1982). Color science: Concepts and methods, quantitative data and formulas. *New York, Wiley*.

Zhou, L., Rzeszotarsk, M. S., Singerman, L. J., and Chokreff, J. M. (1994). The detection and quantification of retinopathy using digital angiograms. *IEEE Transactions on Medical Imaging*, 13.